Effects of short-range nuclear correlations on the deformability of neutron stars

Lucas A. Souza, Mariana Dutra, César H. Lenzi, and Odilon Lourenço
Departamento de Física, Instituto Tecnológico de Aeronáutica, DCTA, 12228-900, São José dos Campos, SP, Brazil

(Received 8 March 2020; revised manuscript received 12 May 2020; accepted 28 May 2020; published 18 June 2020)

In the present work, we investigate the effects of short-range correlations (SRC) on the dimensionless deformability of the binary neutron system related to the GW170817 event. We implemented phenomenological SRC in a relativistic mean-field model in which the bulk parameters, namely, incompressibility (K_0), effective nucleon mass ratio (m^*), symmetry energy (J), and its slope (L_0), are independently controlled. Our results point out that the SRC favor the model to pass through the constraints, established by the LIGO/Virgo Collaboration, on the values of $\Lambda_{1.4}$ and on the $\Lambda_1 \times \Lambda_2$ region. We also found a clear linear correlation between $\Lambda_{1.4}$ with K_0 and L_0 (increasing dependence), and with m^* and J (decreasing dependence). Finally, we also obtained compatible numbers for $R_{1.4}$ (model with and without SRC) in comparison with recent data from the neutron star interior composition explorer mission.

DOI: 10.1103/PhysRevC.101.065202

I. INTRODUCTION

A widely used approach to treat many-nucleon systems (nuclei, for example) is based on the construction of nuclear interactions, such as the one pion exchange potentials, in which the free parameters are adjusted to reproduce, for example, experimental data involved in the simplest bound nuclear system used to study the nucleon-nucleon interaction, namely, the deuteron (proton-neutron pair). This system has a bound state energy of around 2 MeV [1,2], electric quadrupole momentum of 2.82 mb [3], magnetic momentum given by 0.86 mn [4], and is described by a spin 1 and isospin 0 triplet state. From the knowledge of this interaction, it is possible to treat nuclei by using the Brueckner-Hartree-Fock [5,6] method, for example. From another perspective, it is also possible to describe nuclei from the so-called "nuclear shell model" (or "independent particle model") [7], in which it is considered, at first order, that each nucleon moves independently and is affected by an average potential due to the remaining nucleons. From the solution of the Schrödinger equation, the energy levels of the independent nucleon submitted to the average potential $V(r)$ are determined. Possible options for $V(r)$ include the Woods-Saxon potential [8,9], the harmonic oscillator, or even the finite square well potential. In addition, microscopic systems of many interacting particles can be described by approximation methods in which combinations of high-performance computing techniques allow a fundamental understanding of nuclear properties from many-body Hamiltonians. Among the main many-body models, a more fundamental approach compared to the nuclear shell model is the *ab initio* method [10–12]. It is based on the density functional theory (DFT) [13–15] in which many-body correlations are combined to the deuteron and nucleon-nucleon interactions.

The aforementioned many-body approaches present limitations in the mass number such that a current challenge is the search for a universal energy density functional including heavy isotopes, and are able to describe relevant characteristics of finite nuclei and also extended asymmetric nucleonic matter. The shell model is successful, for example, in describing stable nuclei having proton or neutron numbers given by 2, 8, 20, 28, 50, 82, 126 (magic numbers). For these cases, the model predicts nuclei with filled shells. However, electron-induced quasielastic proton knockout experiments [16,17] show that the nucleon-independent particle behavior, in which the shell model is based, occurs to about 70% of nucleons in valence states. Nonindependent nucleons correlate in pairs with high relative momentum due to the short-range components of the nuclear interaction. These correlations are called short-range correlations (SRC) [18–31]. Experiments performed at the Thomas Jefferson National Accelerator Facility (JLab) concluded that for the ^{12}C nucleus, 20% of the nucleons present SRC and, within this set, 90% of the correlated pairs are neutron-proton (np) type [32]. The remaining pairs are divided into 5% for each nn and pp pairs. The experiments consist of very energetic incident electrons in the ^{12}C nucleus. In the collision, it is found that a proton is simultaneously removed with another correlated nucleon, in this case, a neutron more frequently. The dominance of the correlated np pair is also observed in proton removal experiments in heavier nuclei, and even in those with more neutrons, as verified in experiments involving ^{27}Al, ^{56}Fe, and ^{208}Pb [33] nuclei. The predominance of the specific np pair, or in other words, deuteron-like pairs, is justified as a direct consequence of the tensor part of the nuclear interaction [34,35].

The implications of SRC and, more specifically, of the predominance in the np pair formation are diverse, for example, in the analysis of neutrino scattering by correlated nucleons [36,37], in the momentum distribution of the quarks that form these pair [38,39], and also in many nucleon systems such as nuclear matter. Neutron star properties were also shown to be

affected by the inclusion of the SRC phenomenology as one can verify in Ref. [40].

In this work, we focus on the effects of the SRC in the dimensionless tidal deformability (Λ) of the neutron star system related to the GW170817 event [41–48]. Such a recent observation of gravitational waves emission, from the binary neutron star merger event, observed on 17 August 2017, offered an opportunity for a deep understanding of the stellar matter equation of state (EoS), since it provided important constraints that reliable models should satisfy. In Sec. II, we present the structure of the relativistic mean-field (RMF) model, with SRC included, used to obtain the stellar matter EoS and for the calculation of Λ. In Sec. III, we show the influence of the SRC on the deformability of the neutron star binary system. In particular, the results point out that the SRC favor the model to reach the GW170817 constraints. Another interesting result of our study is the clear linear correlations exhibited between the nuclear matter bulk parameters and the deformability. Finally, we present the summary and concluding remarks in Sec. IV.

II. RELATIVISTIC MEAN-FIELD MODEL INCLUDING SHORT-RANGE CORRELATIONS

Probes of the short-range correlations can be verified from the analysis of the nucleon momentum distribution functions in several nuclei [49] such as ^{2}H, ^{4}He, ^{16}O, ^{40}Ca, as well as ^{12}C, ^{56}Fe, and ^{208}Pb, previously mentioned. The SRC imply a decrease in the occupation of the states below the Fermi level and a partial occupation in the states above it. Consequently, the momentum distribution function of nucleons, $n(k)$, is different from the step function of a Fermi gas of independent particles, as depicted in Fig. 1 of Ref. [40], for instance. The marked area in that figure corresponds to the region of the so-called "high momentum tail" (HMT), in which $n(k)$ depends on k as $n(k) \sim k^{-4}$.

In Ref. [40], the authors proposed the implementation of the HMT in the EoS of the relativistic mean field model presenting third and fourth order in the scalar field σ, second and fourth order in the vector field ω, and the interaction between the ρ and ω mesons. Basically, the effect of the HMT is to change the kinetic momentum integrals of the model by replacing the traditional Fermi gas step functions by the new $n(k)$ distributions, in this case, given by $n_{n,p}(k_F, y) = \Delta_{n,p}$ for $0 < k < k_{F\,n,p}$ and $n_{n,p}(k_F, y) = C_{n,p}(k_{F\,n,p}/k)^4$ for $k_{F\,n,p} < k < \phi_{n,p}k_{F\,n,p}$. The proton fraction is given by $y = \rho_p/\rho$ with ρ_p being the proton density, and $\rho = 2k_F^3/(3\pi^2)$ the total one.

In this work, we use the model constructed in Ref. [40] that presents $\Delta_{n,p} = 1 - 3C_{n,p}(1 - 1/\phi_{n,p})$, where $C_p = C_0[1 - C_1(1 - 2y)]$, $C_n = C_0[1 + C_1(1 - 2y)]$, $\phi_p = \phi_0[1 - \phi_1(1 - 2y)]$, and $\phi_n = \phi_0[1 + \phi_1(1 - 2y)]$. Furthermore, we also use $C_0 = 0.161$, $C_1 = -0.25$, $\phi_0 = 2.38$, and $\phi_1 = -0.56$. These values are determined from the analysis of $d(e, e', p)$ reactions, medium-energy photonuclear absorptions, (e, e') reactions, and data from two-nucleon knockout reactions as described in Ref. [50]. The energy density and pressure of the RMF model with SRC implemented from such an approach are, respectively, given by

$$\epsilon = \frac{m_\sigma^2\sigma^2}{2} + \frac{A\sigma^3}{3} + \frac{B\sigma^4}{4} - \frac{m_\omega^2\omega_0^2}{2} - \frac{Cg_\omega^4\omega_0^4}{4} - \frac{m_\rho^2\bar{\rho}_{0(3)}^2}{2} + g_\omega\omega_0\rho + \frac{g_\rho}{2}\bar{\rho}_{0(3)}\rho_3 - \frac{1}{2}\alpha_3' g_\omega^2 g_\rho^2 \omega_0^2 \bar{\rho}_{0(3)}^2 + \epsilon_{\rm kin}^p + \epsilon_{\rm kin}^n \tag{1}$$

and

$$p = -\frac{m_\sigma^2\sigma^2}{2} - \frac{A\sigma^3}{3} - \frac{B\sigma^4}{4} + \frac{m_\omega^2\omega_0^2}{2} + \frac{Cg_\omega^4\omega_0^4}{4} + \frac{m_\rho^2\bar{\rho}_{0(3)}^2}{2} + \frac{1}{2}\alpha_3' g_\omega^2 g_\rho^2 \omega_0^2 \bar{\rho}_{0(3)}^2 + p_{\rm kin}^p + p_{\rm kin}^n \tag{2}$$

with the following kinetic contributions:

$$\epsilon_{\rm kin}^{n,p} = \frac{\gamma\Delta_{n,p}}{2\pi^2}\int_0^{k_{F\,n,p}} k^2 dk (k^2 + M^{*2})^{1/2} + \frac{\gamma C_{n,p}}{2\pi^2}\int_{k_{F\,n,p}}^{\phi_{n,p}k_{F\,n,p}} \frac{k_{F\,n,p}^4}{k^2} dk (k^2 + M^{*2})^{1/2} \tag{3}$$

and

$$p_{\rm kin}^{n,p} = \frac{\gamma\Delta_{n,p}}{6\pi^2}\int_0^{k_{F\,n,p}} \frac{k^4 dk}{(k^2 + M^{*2})^{1/2}} + \frac{\gamma C_{n,p}}{6\pi^2}\int_{k_{F\,n,p}}^{\phi_{n,p}k_{F\,n,p}} \frac{k_{F\,n,p}^4 dk}{(k^2 + M^{*2})^{1/2}}. \tag{4}$$

Since the mean-field approximation is taken, σ, ω_0 (zero component), and $\bar{\rho}_{0_{(3)}}$ (isospin space third component) are the expectation values of the mesons fields in the expressions above. We also use, here, $m_\omega = 782.5$ MeV, $m_\rho = 763$ MeV, and $m_\sigma = 500$ MeV. The effective nucleon mass is defined by $M^* = M_{\rm nuc} - g_\sigma\sigma$, the degeneracy factor is $\gamma = 2$ for asymmetric matter, and $M_{\rm nuc} = 939$ MeV is the nucleon rest mass. The self-consistency of the model imposes on M^* the condition of $M^* - M_{\rm nuc} + (g_\sigma^2/m_\sigma^2)\rho_s - (A/m_\sigma^2)\sigma^2 - (B/m_\sigma^2)\sigma^3 = 0$ with $\rho_s = \rho_{sp} + \rho_{sn}$ and

$$\rho_{sn,p} = \frac{\gamma M^*\Delta_{n,p}}{2\pi^2}\int_0^{k_{F\,n,p}} \frac{k^2 dk}{(k^2 + M^{*2})^{1/2}} + \frac{\gamma M^* C_{n,p}}{2\pi^2}\int_{k_{F\,n,p}}^{\phi_{n,p}k_{F\,n,p}} \frac{k_{F\,n,p}^4}{k^2}\frac{dk}{(k^2 + M^{*2})^{1/2}}. \tag{5}$$

The remaining field equations for ω_0 and $\bar{\rho}_{0(3)}$ are $m_\omega^2\omega_0 = g_\omega\rho - Cg_\omega(g_\omega\omega_0)^3 - \alpha_3' g_\omega^2 g_\rho^2 \bar{\rho}_{0(3)}^2\omega_0$ and $m_\rho^2\bar{\rho}_{0(3)} = g_\rho\rho_3/2 - \alpha_3' g_\omega^2 g_\rho^2 \bar{\rho}_{0(3)}\omega_0^2$.

Six free coupling constants, namely, g_σ, g_ω, g_ρ, A, B, and α_3', are determined in order to reproduce six bulk parameters identified as $\rho_0 = 0.15$ fm^{-3} (saturation density), $B_0 = -16.0$ MeV (binding energy), $m^* \equiv M_0^*/M_{\rm nuc} = 0.60$ (ratio of the effective mass to the nucleon rest mass), $K_0 = 230$ MeV (incompressibility), $J = 31.6$ MeV (symmetry energy), and $L_0 = 58.9$ MeV. Here, one has $B_0 = E(\rho_0) - M$, $M_0^* = M^*(\rho_0)$, $K_0 = 9(\partial p/\partial\rho)_{\rho_0}$, $J = \mathcal{S}(\rho_0)$, and $L_0 = 3\rho_0(\partial\mathcal{S}/\partial\rho)_{\rho_0}$ with $\mathcal{S}(\rho) = (1/8)(\partial^2 E/\partial y^2)|_{y=1/2}$ and $E(\rho) = \epsilon/\rho$.

We remind the reader that the values of the bulk parameters related to the "reference model" applied in Ref. [40] and also in our work are based on different theoretical and experimental studies. Usually, in nuclear mean-field models, saturation density and binding energy are well established closely around the values of 0.15 fm^{-3} and -16.0 MeV, respectively. Regarding the symmetry energy and its slope, the authors of Ref. [51] collected data of these quantities from analyses of different terrestrial nuclear experiments and astrophysical observations. They included investigations of isospin diffusion, neutron skins, pygmy dipole resonances, α and β decays, transverse flow, mass-radius relation, and torsional crust oscillations of neutron stars. From the numbers extracted from these terrestrial laboratory measurements and astrophysical observations, the authors from [51] obtained the average values of $J = 31.6 \pm 2.66$ MeV and $L_0 = 58.9 \pm 16$ MeV. Another set of data analyzed in Ref. [52] provided a similar result for these isovector parameters, namely, $J = 31.7 \pm 3.2$ and $L_0 = 58.7 \pm 28.1$. Concerning the incompressibility, $K_0 = 230$ MeV is consistent with the range of $220\,\mathrm{MeV} \leqslant \mathrm{K}_0 \leqslant 260$ MeV according to the the current consensus on this quantity, see Ref. [53] for instance. Finally, the value of 0.6 for the effective mass ratio is in agreement with the limits of $0.58 \leqslant m^* \leqslant 0.64$ [54]. In Ref. [54], the authors found a strong correlation between m^* and the spin-orbit splittings in nuclei, for a particular class of relativistic models. Theauthors concluded that parametrizations of this model presenting m^* in the mentioned range show spin-orbit splittings in agreement with well-established experimental values for ^{16}O, ^{40}Ca, and ^{208}Pb nuclei. Furthermore, the 263 parametrizations of different kinds of RMF models analyzed in Ref. [55] present a range of $0.52 \leqslant m^* \leqslant 0.80$ for the effective mass ratio. The value of $m^* = 0.6$ used here is also inside this limit.

The last coupling constant of the model, namely, C is chosen to be $C = 0.005$ instead of $C = 0.01$ from Ref. [40]. The former value ensures that the model predicts neutron stars with masses around 2 solar masses (see next section).

In order to complete the equations needed to construct the stellar matter, we present the chemical potentials for protons and neutrons. They are given by

$$\mu_{n,p} = \frac{\partial \epsilon}{\partial \rho_{n,p}} = \mu^{n,p}_{\mathrm{kin(SRC)}} + \Delta_{n,p}\mu^{n,p}_{\mathrm{kin}} + g_\omega \omega_0 \pm \frac{g_\rho}{2}\bar{\rho}_{0_{(3)}} \tag{6}$$

with

$$\mu^{n,p}_{\mathrm{kin}} = \left(k^2_{F\,n,p} + M^{*2}\right)^{1/2} \tag{7}$$

and

$$\mu^{n,p}_{\mathrm{kin\,(SRC)}} = 3C_{n,p}\left[\mu^{n,p}_{\mathrm{kin}} - \frac{\left(\phi^2_{n,p}k^2_{F\,n,p} + M^{*2}\right)^{1/2}}{\phi_{n,p}}\right] + 4C_{n,p}k_{F\,n,p}\ln\left[\frac{\phi_{n,p}k_{F\,n,p} + \left(\phi^2_{n,p}k^2_{F\,n,p} + M^{*2}\right)^{1/2}}{k_{F\,n,p} + \left(k^2_{F\,n,p} + M^{*2}\right)^{1/2}}\right]. \tag{8}$$

In Eq. (6), the sign (+) stands for protons and (−) for neutrons.

From Eqs. (3) and (4) one sees that the SRC induce an extra term in the kinetic contributions of the model. The scalar density, Eq. (5), is also modified in the same direction, and the kinetic part of the chemical potentials of the model changes as $\mu^{n,p}_{\mathrm{kin}} \to \mu^{n,p}_{\mathrm{kin(SRC)}} + \Delta_{n,p}\mu^{n,p}_{\mathrm{kin}}$.

III. RESULTS

A. Stellar matter

In order to determine properties related to the neutron star system, we need to take into account charge neutrality and β-equilibrium conditions. We consider stellar matter composed by protons, neutrons, electrons, and muons with the last leptons emerging when the electron chemical potential exceeds the muon mass, i.e., for $\mu_e = (3\pi^2\rho_e)^{1/3} > m_\mu = 105.7$ MeV (ρ_e is the electron density). Such assumptions lead to the constraints given by $\mu_n - \mu_p = \mu_e = \mu_\mu$ and $\rho_p - \rho_e = \rho_\mu = [(\mu^2_\mu - m^2_\mu)^{3/2}]/(3\pi^2)$, which have to be coupled to the field equations coming from the RMF model. The chemical potential and density for the muons are given, respectively, by μ_μ and ρ_μ. The total energy density and pressure of stellar matter are $\mathcal{E} = \epsilon + \epsilon_e + \epsilon_\mu$ and $P = p + p_e + p_\mu$, respectively, with ϵ_l and p_l being the energy density and pressure of the lepton $l = e, \mu$. Some neutron star properties, such as mass-radius profile, can be found by solving the Tolman-Oppenheimer-Volkoff (TOV) equations [56,57].

The spherically symmetric neutron star is composed of a core, described here by the RMF model previously presented along with the leptons considered, and a crust, divided into outer and inner parts. Due to the restricted knowledge about this specific part of the neutron star (there is not a consensus with regard to its exact composition), we decided to treat this region with widely used approaches without further assumptions, i.e., without the inclusion of possible SRC effects. Moreover, the main purpose of our study is to analyze the effects of SRC on $\Lambda_{1.4}$ and, according to Ref. [59], the more important contribution for this quantity comes from the neutron star core EoS, in which we implement the SRC phenomenology. We model the outer crust by the Baym-Pethick-Sutherland (BPS) equation of state [58] in the density region of $6.3 \times 10^{-12}\,\mathrm{fm}^{-3} \leqslant \rho \leqslant 2.5 \times 10^{-4}\,\mathrm{fm}^{-3}$ [59,60]. For the inner part, we use the polytropic form given by $P(\mathcal{E}) = A + B\mathcal{E}^{4/3}$ [40,59,61,62] in a range of $2.5 \times 10^{-4}\,\mathrm{fm}^{-3} \leqslant \rho \leqslant \rho_\mathrm{t}$, where ρ_t is the density associated to the core-crust transition found, in our case, by the thermodynamical method [63–66].

For both versions of the model, namely, with and without SRC included, we found a maximum neutron star mass of $M_{\max} = 2.05M_\odot$ and $M_{\max} = 1.96M_\odot$, respectively. All of them are compatible with the limits of $(1.928 \pm 0.017)M_\odot$ [67,68], $(2.01 \pm 0.04)M_\odot$ [69], $2.14^{+0.20}_{-0.18}M_\odot$ (95.4% credible level) [70], and $2.14^{+0.10}_{-0.09}M_\odot$ (68.3% credible level) [70]. It is worth noticing that the effect of increasing $M_{\max}$ pointed out in Ref. [40], which uses $C = 0.01$, is also obtained in our model, in which $C = 0.005$. In Fig. 1, we display the mass-radius profile obtained

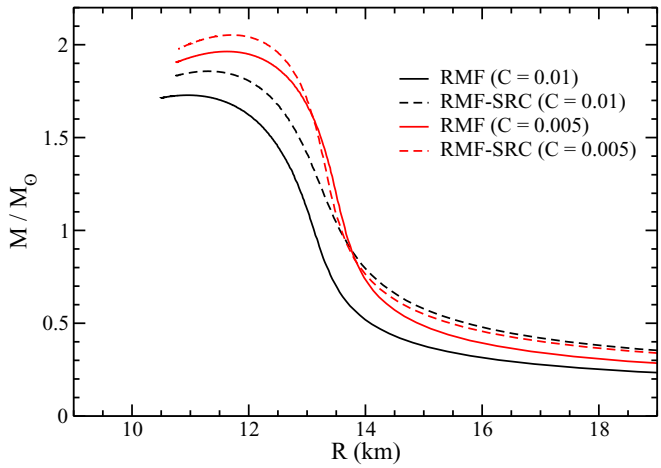

FIG. 1. Mass-radius diagram for the RMF and RMF-SRC models for $C = 0.01$ (black curves) and 0.005 (red curves).

from the RMF model, with (RMF) and without (RMF-SRC) SRC effects, for $C = 0.01$ (used in Ref. [40]), and for $C = 0.005$ (used in this work). Notice the difference in $M_{\rm max}$ in both parametrizations due to the reduction of the quartic-self-coupling strength (C parameter) of the repulsive vector field ω.

We are not restricted here to the reference model, namely, the one with the bulk parameters given by $\rho_0 = 0.15$ fm^{-3}, $B_0 = -16.0$ MeV, $m^* = 0.60$, $K_0 = 230$ MeV, $J = 31.6$ MeV, and $L_0 = 58.9$ MeV, for $C = 0.005$. We also generate different parametrizations by changing only one of these quantities while keeping the other ones fixed. We calculate, for RMF and RMF-SRC models, some properties related to the maximum mass neutron star for a set of different parametrizations. The results are depicted in Fig. 2, namely, maximum mass ($M_{\rm max}$), radius ($R_{\rm max}$), and central energy density ($\mathcal{E}_{\rm cmax}$). The transition densities (ρ_t), obtained for all the parametrizations studied, are shown as well.

As one can see all parametrizations, constructed through the variation of the bulk parameters, present $M_{\rm max}$ compatible with the observation of $2M_\odot$ ms pulsars, except for those in which $m^* \geqslant 0.65$ (RMF model). Furthermore, regarding the effect of the SRC on the maximum mass, we see that such a phenomenology contributes to increase this quantity, as also shown in Fig. 1. In the case of m^* variation, this increasing is reduced as m^* approaches to 0.65. One can also notice a reduction of $M_{\rm max}$ with m^* in both models, a feature also registered in Ref. [71]. Another interesting result concerning the inclusion of SRC is the reduction of the ρ_t values. This means that the SRC enlarge the thermodynamical stable region described by the RMF-SRC model in comparison with the RMF one.

B. Deformability calculations (GW170817 event)

Since the main quantities regarding the stellar matter description are determined, we now focus on the deformability calculation related to the neutron star binary system studied

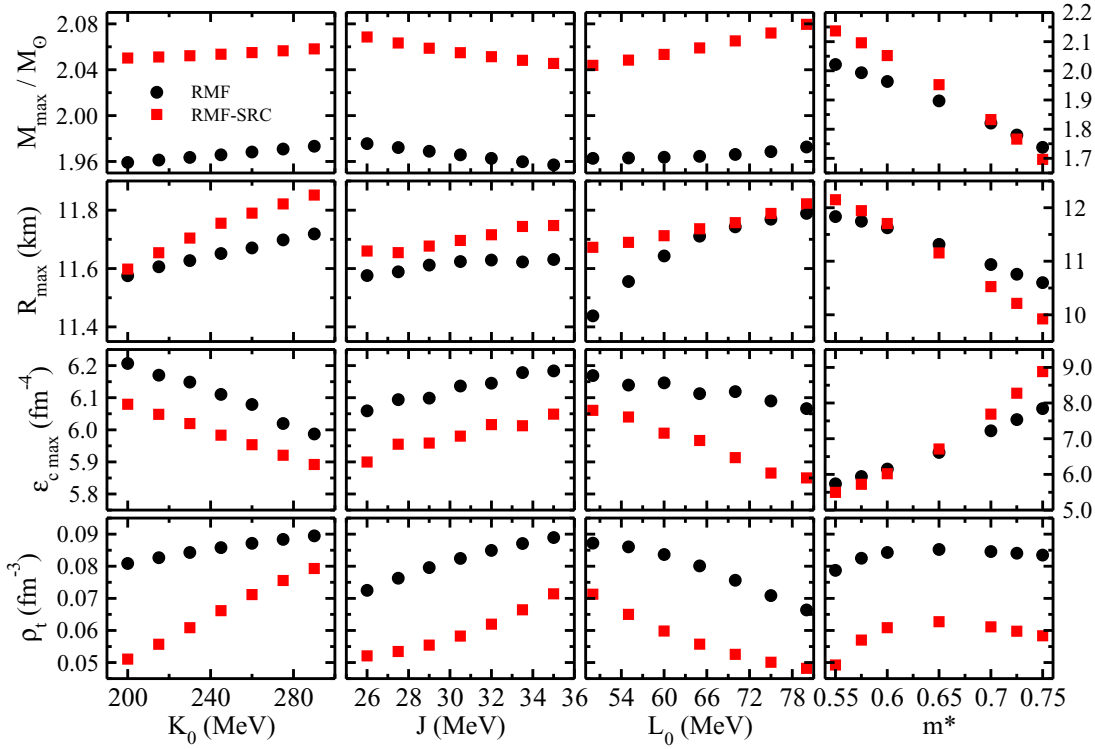

FIG. 2. Transition density (ρ_t) and stellar matter quantities related to the neutron star with maximum mass, namely, the maximum mass over $M_\odot$ ($M_{\rm max}/M_\odot$), radius ($R_{\rm max}$), and central energy density ($\mathcal{E}_{\rm cmax}$), as a function of the bulk parameters.

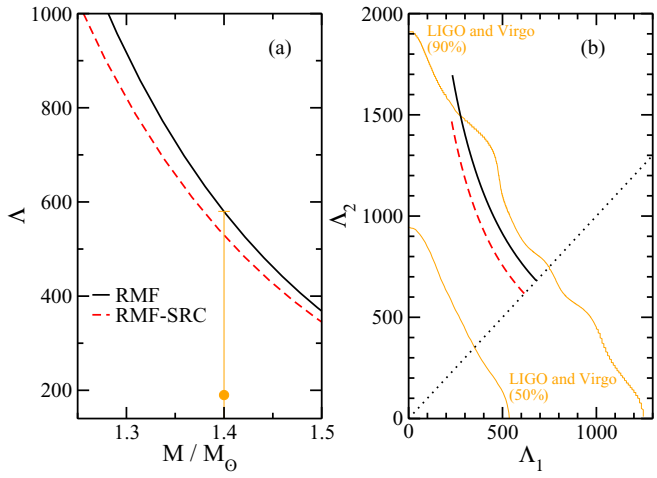

FIG. 3. Results from the model with (RMF-SRC) and without (RMF) SRC effects. (a) Λ as a function of M. Full circle: result of $\Lambda_{1.4} = 190^{+390}_{-120}$ from Ref. [42]. (b) Dimensionless tidal deformabilities for the case of high-mass (Λ_1) and low-mass (Λ_2) components of the GW170817 event. The confidence lines (90% and 50%) are also taken from Ref. [42].

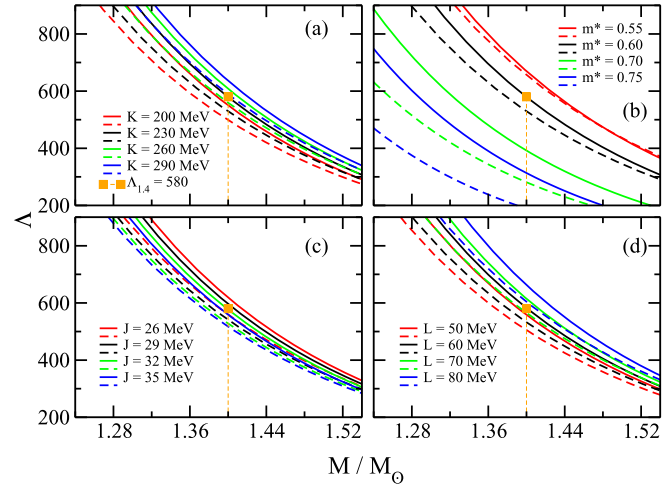

FIG. 4. Λ as a function of the neutron star mass for different parametrizations of the RMF model with (dashed lines) and without (full lines) SRC included. Orange square: upper limit of $\Lambda_{1.4} = 190^{+390}_{-120}$.

in the GW170817 event [41–43]. For this purpose, we need to obtain the dimensionless tidal deformability, written in terms of the (second) tidal Love number k_2 as $\Lambda = 2k_2/(3C^5)$ with $C = M/R$ (M and R are the mass and radius, respectively, of the neutron star). k_2 is evaluated through the following expression:

$$\begin{aligned} k_2 = {} & \frac{8C^5}{5}(1-2C)^2[2+2C(y_R-1)-y_R] \\ & \times\{2C[6-3y_R+3C(5y_R-8)] \\ & +4C^3[13-11y_R+C(3y_R-2)+2C^2(1+y_R)] \\ & +3(1-2C)^2[2-y_R+2C(y_R-1)]\ln(1-2C)\}^{-1} \quad (9) \end{aligned}$$

with $y_R \equiv y(R)$. The function $y(r)$ is obtained through the solution of a differential equation solved as part of a coupled system of equations containing the TOV ones [59,72–76].

In Fig. 3, we show the results of Λ as a function of the neutron star mass and the dimensionless deformabilities related to the binary system of the GW170817 event. For the sake of comparison, we display results for the model with and without short-range correlations included. From the figure, it is clear that SRC favor the model to reach the GW170817 data, since $\Lambda_{1.4}$ decreases in comparison with the model without the effects, see panel (a), and the $\Lambda_2 \times \Lambda_1$ curve moves to the direction of the inner region of the LIGO and Virgo Collaboration (LVC) data, as can be seen in panel (b). In the calculations of Fig. 3(b), we use the range of $1.365 \leqslant m_1/M_\odot \leqslant 1.60$ [41] for the neutrons star with mass m_1 from the binary system, and the corresponding mass of the companion star, obtained through $[(m_1m_2)^{3/5}]/[(m_1+m_2)^{1/5}] = 1.188M_\odot$ [41].

We also verified whether the SRC effects are restricted or not to the reference model used in this work, by generating different parametrizations obtained from the independent variation of each bulk parameter. In that way, we ensure the particular effect of the specific quantity we are changing. In Figs. 4 and 5 we display the results for such new parametrizations.

For example, in Figs. 4(a) and 5(a) we generate four parametrizations, each one with $\rho_0 = 0.15$ fm^{-3}, $B_0 = -16.0$ MeV, $m^* = 0.60$, $J = 31.6$ MeV, and $L_0 = 58.9$ MeV fixed, but changing K_0 as indicated in the panels. For each particular parametrization, we tested the effect of the SRC. The same procedure is performed for the other isoscalar and isovector bulk parameters in the remaining panels. The results show the same behavior presented in Fig. 3, i.e., the SRC affects the dimensionless deformabilities, namely, $\Lambda_{1.4}$ and the Λ_1-Λ_2 pair, always in the direction of the LVC observational data. The smaller effect of the SRC inclusion is observed for the parametrization for which $m^* = 0.55$. Nevertheless, it is also observed that the SRC effects are more pronounced for parametrizations with higher values of m^*. Notice that

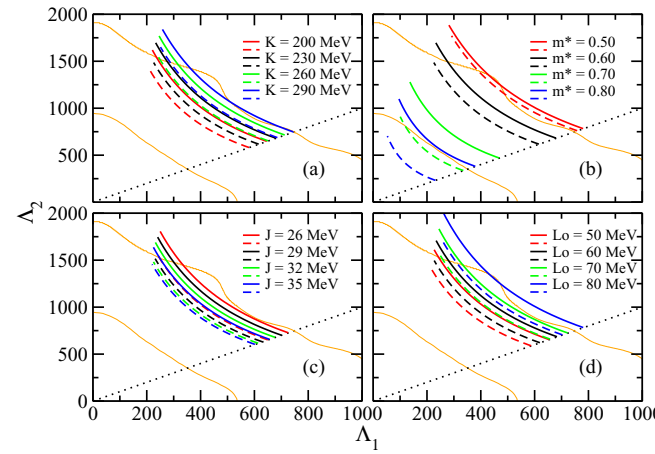

FIG. 5. $\Lambda_1 \times \Lambda_2$ for different parametrizations of the RMF model with (dashed lines) and without (full lines) SRC included. Orange lines: confidence lines of 90% and 50% from Ref. [42].

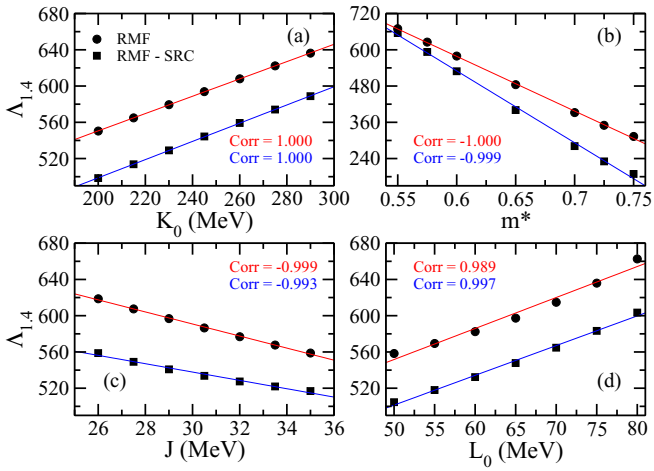

FIG. 6. $\Lambda_{1.4}$ as a function of the bulk parameters: (a) K_0, (b) m^*, (c) J, and (d) L_0. Results for the model with (squares) and without (circles) short-range correlations included. Full lines: fitting curves.

the differences between the models with and without SRC are higher for parametrizations with $m^* \geqslant 0.60$. Since $M^* = M_{\rm nuc} - g_\sigma \sigma$, it is possible to say that the attractive interaction, represented by the scalar σ field, plays the major role regarding the effects produced by the inclusion of the SRC in the model. Such a feature is verified in the deformability calculations.

Since we are able to generate different parametrizations of the RMF model by changing independently its bulk parameters, we performed an investigation on the impact of these quantities in the dimensionless deformability related to the canonical star ($M = 1.4M_\odot$), namely, $\Lambda_{1.4}$. The results are depicted in Fig. 6. For all parametrizations, $\rho_0 = 0.15$ fm^{-3} and $B_0 = -16.0$ MeV are fixed. From the figure, one can notice a clear linear correlation between $\Lambda_{1.4}$ and the bulk parameters with correlation coefficients around 1. Such relationships are preserved even when the SRC are included in the model. For this case, it is observed that this phenomenology favors the model to reach the limits of $\Lambda_{1.4} = 190^{+390}_{-120}$ from the LVC, corroborating the findings exhibited in Fig. 4. Furthermore, it is also clear that $\Lambda_{1.4}$ is more sensitive to variations of m^*, as we discussed above. Such a pattern is confirmed in Fig. 6(b) with a linear dependence clearly established. We also notice that $\Lambda_{1.4}$ is an increasing function of K_0 or L_0, and decreases with J or m^*. This feature is also presented for the parametrizations of the RMF-SRC model. Regarding the L_0 dependence of $\Lambda_{1.4}$, it is worth noticing that such a pattern (increasing of $\Lambda_{1.4}$ with L_0) was also observed in Ref. [77], in which the authors used the empirical parabolic law for the energy per particle as a function of the density and the isospin asymmetry $\delta = 1 - 2y$. Their findings and ours can be indicative that the $\Lambda_{1.4} \times L_0$ function may follow an increasing behavior, and as we have shown, the SRC do not break this pattern.

Other interesting results, obtained from the analysis of Fig. 6, are the ranges of the bulk parameters extracted from the relationships of these quantities with the limits of $\Lambda_{1.4} = 190^{+390}_{-120}$. Since K_0 and L_0 can be negatives, from the linear fitting curves, we focus on their maximum values, related to the upper limit of $\Lambda_{1.4}$. They are given by 230 MeV and 58 MeV, respectively, for the RMF model. On the other hand, when SRC are included, these numbers change to $K_0 = 280$ MeV and $L_0 = 74$ MeV. For the incompressibility, some overlap is found for these ranges (with and without SRC) and the current consensus of $220\,\text{MeV} \leqslant \text{K}_0 \leqslant 260$ MeV [53]. Concerning L_0, an intersection is also found with the range of $25\,\text{MeV} \leqslant \text{L}_0 \leqslant 115$ MeV [55], or even the more stringent ones given by $L_0 = 58.9 \pm 16$ MeV [40] and $L_0 = 58.7 \pm 28.1$ MeV [52], for instance. For both quantities, it is verified that the SRC enlarge the overlaps between the values of K_0 and L_0 estimated from the LVC data and the ones found by other predictions. Concerning the limits of J and m^*, the fitting curves do not produce negative values for these quantities. For the symmetry energy, the limits found are quite large, namely, $31.6\,\text{MeV} \leqslant \text{J} \leqslant 108$ MeV (RMF) and $20.8\,\text{MeV} \leqslant \text{J} \leqslant 131$ MeV (RMF-SRC), in comparison with $J = 31.6 \pm 2.66$ MeV [40], $J = 31.7 \pm 3.2$ MeV [52], and $25\,\text{MeV} \leqslant \text{J} \leqslant 35$ MeV [55]. For the effective mass, the ranges are given by $0.60 \leqslant m^* \leqslant 0.88$ and $0.58 \leqslant m^* \leqslant 0.79$, respectively, for the RMF model and the RMF-SRC one. Unlike the ranges of K_0, L_0, and J, the SRC reduce the range of m^* obtained through the association with $\Lambda_{1.4} = 190^{+390}_{-120}$.

As a remark, we emphasize to the reader that the effect of the bulk parameters on $\Lambda_{1.4}$ displayed in Fig. 6 (increasing or decreasing, at least) is not universal concerning all quantities, namely, K_0, m^*, J, and L_0. In Ref. [46], for instance, it was observed that $\Lambda_{1.4}$ increases as a function of K_0 in a density dependent van der Waals model (nucleon-nucleon interactions parametrized as a function of the density). This is the same pattern observed in the RMF/RMF-SRC models. However, in that model $\Lambda_{1.4}$ increases as J increases, showing the opposite behavior in comparison with Fig. 6(c). Furthermore, this opposite dependence is also presented in the RMF/RMF-SRC models in which $C = \alpha_3' = 0$ in Eqs. (1) and (2) (not shown). For these models, there is no restriction on the symmetry energy slope as in the models studied here. With regard to the m^* dependence of $\Lambda_{1.4}$, decreasing the latter as a function of the former is also observed in Ref. [71], where the authors investigate a RMF model with $C = 0$. Lastly, the effect of L_0 is also shown to be increasing in $\Lambda_{1.4}$ for nonrelativistic Gogny and MDI models studied in Ref. [48]. In this reference, the authors also found a clear linear correlation for $\Lambda_{1.4} \times L_0$. The increasing of $\Lambda_{1.4}$ due to the increasing of L_0 was also verified in Refs. [77,78].

Finally, by restricting our calculations to the ranges for K_0, L_0, J, and m^* given by the circles and squares presented in Fig. 6, we obtained the following results for the radius of the neutron star with $M \sim 1.4M_\odot$: $12.45\,\text{km} \leqslant \text{R}_{1.4} \leqslant 13.71\,\text{km}$ (RMF) and $11.51\,\text{km} \leqslant \text{R}_{1.4} \leqslant 13.61\,\text{km}$ (RMF-SRC). Such limits are in agreement with the recent findings related to the millisecond pulsar PSR J0030 + 0451, namely, $R_{1.4} = 13.89^{+1.22}_{-1.39}$ km [79] and $R_{1.4} = 13.02^{+1.24}_{-1.06}$ km [80], determined from the data coming from the NASA Neutron Star Interior Composition Explorer (NICER) mission.

IV. SUMMARY AND CONCLUDING REMARKS

In this work we analyzed the effects of the short-range correlations (SRC) on the dimensionless deformability related to the binary neutron star system of the GW170817 event. For the RMF model used in this work, in which $\rho_0 = 0.15$ fm^{-3}, $B_0 = -16.0$ MeV, $m^* = 0.60$, $K_0 = 230$ MeV, $J = 31.6$ MeV, and $L_0 = 58.9$ MeV, we verified that the inclusion of the SRC favor the model to reach the constraint of $\Lambda_{1.4} = 190^{+390}_{-120}$ (regarding the neutron star of $M = 1.4M_\odot$) and that one observed in the $\Lambda_1 \times \Lambda_2$ region, as we show in Fig. 3. This feature is not restricted to this particular model. We verified that the impact of the SRC is the same even for different parametrizations (different bulk parameters), as exhibited in Figs. 4 and 5. The SRC are more pronounced with respect to variations of m^*, which shows a more important role of the attractive interaction represented by the scalar field σ.

We also analyzed that $\Lambda_{1.4}$ is strongly correlated with the isoscalar quantities K_0 and m^*, and the isovector ones J and L_0. The relationships remain the same, i.e., a linear dependence, even when SRC are included, according to the findings pointed out in Fig. 6. It was also verified that the ranges for the bulk parameters, associated with $\Lambda_{1.4} = 190^{+390}_{-120}$, present some overlap with other constraints on K_0, J, and L_0 obtained from different predictions. Finally, the calculations with the RMF and RMF-SRC models pointed out compatible numbers for $R_{1.4}$ in comparison with the data obtained from the NICER mission.

ACKNOWLEDGMENTS

This work is a part of the project INCT-FNA Proc. No. 464898/2014-5, partially supported by Conselho Nacional de Desenvolvimento Científico e Tecnológico (CNPq) under Grants No. 310242/2017-7 and No. 406958/2018-1 (O.L.), No. 433369/2018-3 (M.D.), and by Fundação de Amparo à Pesquisa do Estado de São Paulo (FAPESP) under the thematic Projects No. 2013/26258-4 (O.L.), 2019/07767-1 (L.A.S.), and No. 2017/05660-0 (O.L., M.D.). L.A.S. thanks the support by INCT-FNA Proc. No. 88887.464764/2019-00.

[1] R. Wilson, *The Nucleon-Nucleon Interaction* (Interscience, New York, 1963).
[2] J. H. E. Mattauch, W. Thiele, and A. H. Wapstra, Nucl. Phys. **67**, 1 (1965).
[3] G. P. Auffray, Phys. Rev. Lett. **6**, 120 (1961).
[4] I. Lindgren, *Alpha-, Beta-, and Gamma-Ray Spectroscopy* (North-Holland, Amsterdam, 1966).
[5] P. Ring and P. Schuck, *The Nuclear Many-Body Problem* (Springer-Verlag, Berlin, 2000).
[6] H. A. Bethe, Annu. Rev. Nucl. Sci. **21**, 93 (1971).
[7] K. L. G. Heyde, *The Nuclear Shell Model*, 2nd ed. (Springer-Verlag, Berlin/Heidelberg, 1994).
[8] R. D. Woods and D. S. Saxon, Phys. Rev. **95**, 577 (1954).
[9] E. Rost, Phys. Lett. B **26**, 184 (1968).
[10] S. Pastore, J. Carlson, V. Cirigliano, W. Dekens, E. Mereghetti, and R. B. Wiringa, Phys. Rev. C **97**, 014606 (2018).
[11] P. Navrátil and E. Caurier, Phys. Rev. C **69**, 014311 (2004).
[12] C. Forssén, P. Navrátil, W. E. Ormand, and E. Caurier, Phys. Rev. C **71**, 044312 (2005).
[13] J. Erler, C. J. Horowitz, W. Nazarewicz, M. Rafalski, and P.-G. Reinhard, Phys. Rev. C **87**, 044320 (2013).
[14] N. Schunck, *Energy Density Functional Methods for Atomic Nuclei* (IoP Publishing, Bristol, 2019).
[15] A. Bulgac, Annu. Rev. Nucl. Part. Sci. **63**, 97 (2013).
[16] L. Lapikas, Nucl. Phys. A **553**, 297 (1993).
[17] J. J. Kelly, Adv. Nucl. Phys. **23**, 75 (1996).
[18] M. Duer, O. Hen, E. Piasetzky *et al.*, Nature **560**, 617 (2018).
[19] O. Hen, G. A. Miller, E. Piasetzky, and L. B. Weinstein, Rev. Mod. Phys. **89**, 045002 (2017).
[20] Z. Ye and J. Arrington, arXiv:1810.03667 (2018).
[21] K. S. Egiyan *et al.* (CLAS Collaboration), Phys. Rev. Lett. **96**, 082501 (2006).
[22] L. L. Frankfurt, M. I. Strikman, D. B. Day, and M. Sargsyan, Phys. Rev. C **48**, 2451 (1993).
[23] N. Fomin *et al.*, Phys. Rev. Lett. **108**, 092502 (2012).
[24] C. C. degli Atti, Phys. Rep. **590**, 1 (2015).
[25] R. Shneor *et al.*, Phys. Rev. Lett. **99**, 072501 (2007).
[26] A. Tang, J. W. Watson, J. Aclander, J. Alster, G. Asryan, Y. Averichev *et al.*, Phys. Rev. Lett. **90**, 042301 (2003).
[27] Z. Li, Z. Ren, B. Hong, H. Lu, and D. Bai, Nucl. Phys. A **990**, 118 (2019).
[28] B. Schmookler, M. Duer, A. Schmidt *et al.* (CLAS Collaboration), Nature **566**, 354 (2019).
[29] M. Duer, O. Hen, E. Piasetzky *et al.*, Phys. Lett. B **797**, 134792 (2019).
[30] J. Ryckebusch, W. Cosyn, T. Vieijra, and C. Casert, Phys. Rev. C **100**, 054620 (2019).
[31] J.-W. Chen, W. Detmold, J. E. Lynn, and A. Schwenk, Phys. Rev. Lett. **119**, 262502 (2017).
[32] R. Subedi *et al.*, Science **320**, 1476 (2008).
[33] O. Hen *et al.*, Science **346**, 614 (2014).
[34] R. Schiavilla, R. B. Wiringa, S. C. Pieper, and J. Carlson, Phys. Rev. Lett. **98**, 132501 (2007).
[35] M. M. Sargsian, T. V. Abrahamyan, M. I. Strikman, and L. L. Frankfurt, Phys. Rev. C **71**, 044615 (2005).
[36] L. Fields *et al.*, Phys. Rev. Lett. **111**, 022501 (2013).
[37] G. A. Fiorentini *et al.*, Phys. Rev. Lett. **111**, 022502 (2013).
[38] O. Hen, D. W. Higinbotham, G. A. Miller, E. Piasetzky, and L. B. Weinstein, Int. J. Mod. Phys. E **22**, 1330017 (2013).
[39] L. B. Weinstein, E. Piasetzky, D. W. Higinbotham, J. Gomez, O. Hen, and R. Shneor, Phys. Rev. Lett. **106**, 052301 (2011).
[40] B. J. Cai and B. A. Li, Phys. Rev. C **93**, 014619 (2016).
[41] B. P. Abbott *et al.* (LIGO Scientific Collaboration and Virgo Collaboration), Phys. Rev. Lett. **119**, 161101 (2017).
[42] B. P. Abbott *et al.* (LIGO Scientific Collaboration and Virgo Collaboration), Phys. Rev. Lett. **121**, 161101 (2018).
[43] B. P. Abbott *et al.* (LIGO Scientific Collaboration and Virgo Collaboration), Phys. Rev. X **9**, 011001 (2019).
[44] A. G. Chaves and T. Hinderer, J. Phys. G **46**, 123002 (2019).
[45] O. Lourenço, M. Dutra, C. H. Lenzi, C. V. Flores, and D. P. Menezes, Phys. Rev. C **99**, 045202 (2019).
[46] O. Lourenço, M. Dutra, C. H. Lenzi, M. Bhuyan, S. K. Biswal, and B. M. Santos, Astrophys. J. **882**, 67 (2019).

[47] O. Lourenço, M. Dutra, C. H. Lenzi, S. K. Biswal, M. Bhuyan, and D. P. Menezes, Eur. Phys. J. A **56**, 32 (2020).
[48] O. Lourenço, M. Bhuyan, C. H. Lenzi, M. Dutra, C. Gonzalez-Boquera, M. Centelles, and X. Viñas, Phys. Lett. B **803**, 135306 (2020).
[49] J. Arrington, D. W. Higinbotham, G. Rosner, and M. Sargsian, Prog. Part. Nucl. Phys. **67**, 898 (2012).
[50] B. J. Cai and B.-A. Li, Phys. Rev. C **92**, 011601(R) (2015).
[51] B.-A. Li and Xiao Han, Phys. Lett. B **727**, 276 (2013).
[52] M. Oertel, M. Hempel, T. Klähn, and S. Typel, Rev. Mod. Phys. **89**, 015007 (2017).
[53] U. Garg and G. Colò, Prog. Part. Nucl. Phys. **101**, 55 (2018).
[54] R. J. Furnstahl, John J. Rusnak, and Brian D. Serot, Nucl. Phys. A **632**, 607 (1998).
[55] M. Dutra, O. Lourenço, S. S. Avancini, B. V. Carlson, A. Delfino, D. P. Menezes, C. Providência, S. Typel, and J. R. Stone, Phys. Rev. C **90**, 055203 (2014).
[56] R. C. Tolman, Phys. Rev. **55**, 364 (1939).
[57] J. R. Oppenheimer and G. M. Volkoff, Phys. Rev. **55**, 374 (1939).
[58] G. Baym, C. Pethick, and P. Sutherland, Astrophys. J. **170**, 299 (1971).
[59] J. Piekarewicz and F. J. Fattoyev, Phys. Rev. C **99**, 045802 (2019).
[60] T. Malik, B. K. Agrawal, J. N. De, S. K. Samaddar, C. Providência, C. Mondal, and T. K. Jha, Phys. Rev. C **99**, 052801(R) (2019).
[61] J. Carriere, C. Horowitz, and J. Piekarewicz, Astrophys. J. **593**, 463 (2003).
[62] C. Gonzalez-Boquera, M. Centelles, X. Viñas, and L. M. Robledo, Phys. Lett. B **779**, 195 (2018).
[63] C. Gonzalez-Boquera, M. Centelles, X. Viñas, and A. Rios, Phys. Rev. C **96**, 065806 (2017).
[64] J. Xu, L.-W. Chen, B.-A. Li, and H.-R. Ma, Astrophys. J. **697**, 1549 (2009).
[65] S. Kubis, Phys. Rev. C **70**, 065804 (2004).
[66] C. Gonzalez-Boquera, M. Centelles, X. Viñas, and T. R. Routray, Phys. Rev. C **100**, 015806 (2019).
[67] E. Fonseca, T. T. Pennucci, J. A. Ellis, I. H. Stairs, D. J. Nice *et al.*, Astrophys. J. **832**, 167 (2016).
[68] P. B. Demorest, T. Pennucci, S. M. Ransom, M. S. E. Roberts, and J. W. T. Hessels, Nature **467**, 1081 (2010).
[69] J. Antoniadis, P. C. C. Freire, N. Wex *et al.*, Science **340**, 1233232 (2013).
[70] H. T. Cromartie *et al.*, Nat. Astron. Lett. **4**, 72 (2020).
[71] N. Hornick, L. Tolos, A. Zacchi, J. E. Christian, and J. Schaffner-Bielich, Phys. Rev. C **98**, 065804 (2018).
[72] T. Hinderer, B. D. Lackey, Ryan N. Lang, and J. S. Read, Phys. Rev. D **81**, 123016 (2010).
[73] S. Postnikov, M. Prakash, and J. M. Lattimer, Phys. Rev. D **82**, 024016 (2010).
[74] T. Hinderer, Astrophys. J. **677**, 1216 (2008).
[75] T. Damour and A. Nagar, Phys. Rev. D **81**, 084016 (2010).
[76] T. Binnington and E. Poisson, Phys. Rev. D **80**, 084018 (2009).
[77] N.-B. Zhang, and Bao-An Li, J. Phys. G **46**, 014002 (2019).
[78] P. G. Krastev and Bao-An Li, J. Phys. G **46**, 074001 (2019).
[79] G. Raaijmakers *et al.*, Astrophys. J. Lett. **887**, L22 (2019).
[80] M. C. Miller *et al.*, Astrophys. J. Lett. **887**, L24 (2019).